Research Square

Preprints are preliminary reports that have not undergone peer review.
They should not be considered conclusive, used to inform clinical practice,
or referenced by the media as validated information.

The effect of titanium dioxide nanoparticles on the structure and electrochemical properties of a PVDF/PSF composite polymer electrolyte for Li-metal battery

Igor V. Gumennyi

gumennyy@ips.ac.ru

A.V. Topchiev Institute of Petrochemical Synthesis

Alexander V. Babkin

Lomonosov Moscow State University

Vitaly A. Govorov

Moscow Power Engineering Institute

Alexander Ya. Malkin

A.V. Topchiev Institute of Petrochemical Synthesis

Vladimir G. Sergeyev

Lomonosov Moscow State University

Research Article

Keywords:

Posted Date: April 17th, 2026

DOI: https://doi.org/10.21203/rs.3.rs-9084725/v1

License: This work is licensed under a Creative Commons Attribution 4.0 International License.
Read Full License

Additional Declarations: No competing interests reported.

ARTICLE

The effect of titanium dioxide nanoparticles on the structure and electrochemical properties of a PVDF/PSF composite polymer electrolyte for Li-metal battery†

Received 00th January 20xx,
Accepted 00th January 20xx

DOI: 10.1039/x0xx00000x

Gumennyi Igor Vladimirovich*[a], Babkin Alexander Vladimirovich[b], Govorov Vitaly Alexandrovich[c], Malkin Alexander Yakovlevich[a], Sergeyev Vladimir Glebovich[b]

A composite polymer electrolyte system based on a polyvinylidene fluoride/polysulfone (PVDF/PSF) mixture with perchlorate lithium salt ($LiClO_4$) and dispersed titanium dioxide nanoparticles in different concentrations was studied. Structural studies were performed using X-ray diffraction (XRD), Fourier transform infrared spectroscopy (FTIR) and scanning electron microscopy (SEM). Electrochemical analysis of the composite films showed that the ionic conductivity increased with the content of titanium dioxide particles, reached a peak at about 10-15 wt. %. After this point, conductivity began to decrease. The effect of increased ion conductivity on temperature was also investigated. A maximum ionic conductivity of 1.5×10^{-5} Sm/cm was achieved at a 10 wt. % concentration of nanoparticles in the composite polymer electrolyte at room temperature. However, preheating the film up to 80°C increased the value of ionic conductivity by three times (when comparing systems with and without nanoparticles) at the same temperature. The LFP//PVDF/PSF/TiO_2//Li cells exhibited excellent rate capability – 149 mAh/g at C/5 rate.

Introduction

Rechargeable batteries are a crucial technology for storing energy in a wide range of applications. Every year, research in this field leads to an increase in the number of battery-powered devices, such as electric vehicles and different types of portable electronics. Lithium-ion batteries are stand out among rechargeable batteries due to their potential for efficient energy storage[1,2]. However, the current state of lithium-ion battery development falls short of the rapidly growing demands [3].

There are two main challenges that hinder development: firstly, advanced batteries based on nickel–cobalt–manganese/graphite components have a low energy density (approximately 200-300 Wh/kg) and a narrow operating temperature range (20–60 °C)[4], which limits their long-term use [5], as well as a short service life. Secondly, there is an increasing problem with battery fires and explosions. Laptops and other devices that use lithium-ion batteries are often linked to fire-related accidents [6]. These issues are directly related to the use of organic liquid electrolytes [7,8].

In addition, the growing demand for convenient personal electronic devices has resulted in the development of flexible and wearable technologies, such as foldable displays and flexible phones. These devices need to be able to function reliably despite significant mechanical stress [9].

To solve these problems, it was proposed in the 1980s to replace liquid electrolytes with solid polymer electrolytes (SPE) [10]. Solid-state electrolytes have several advantages over liquid electrolytes, such as electrochemical stability, a wider operating temperature range, higher energy density and lack of leakage. These features make them excellent candidates for next-generation battery technology [11]. Additionally, the absence of a liquid component in SPE can reduce production costs and allow for a wider variety of shapes and increased cell density.

Despite some success, polymer-based electrolyte systems still exhibit significantly lower ionic conductivity and lower mechanical strength compared to liquid and ceramic electrolytes at room temperature [12]. There are various methods aimed at addressing these challenges, including [13–17]: (a) blending two polymers, (b) adding plasticizers, (c) incorporating inorganic nanoparticles, and (d) modifying the polymer structure. However, a more holistic approach is required to address these issues simultaneously.

A semicrystalline polyvinylidene fluoride (PVDF) was chosen as the polymer matrix in this study. PVDF has a promising material for solid polymer electrolytes, as it exhibits good

[a] A.V. Topchiev Institute of Petrochemical Synthesis, Russian Academy of sciences, Russia, 119991, Moscow, 29 Leninsky prospect. gumennyy@ips.ac.ru
[b] Department of Chemistry, M.V. Lomonosov Moscow State University Russia, 119991, Moscow, Leninskie Gory.
[c] National Research University "Moscow Power Engineering Institute", Russia, 111250, Moscow, Krasnokazarmennaya 17.

† Supplementary information available: 1. Rationale for the selection of polymer ratio; figure s.1. Investigation of the impact of PSF on the ionic conductivity of a polymer film based PVDF. 2. Dispersion of titanium dioxide within a polymer film utilizing various dispersants; figure s.2 Quantitative distribution of titanium in polymer films with different dispersants: a, b) film without dispersant; c, d) BYK 185. On the left – spectra along the characteristic radiation line of titanium, on the right – Fourier transform; figure s.3. Distribution of sulfur in sections of films with different titanium dioxide content. 3. Formulae for calculating phase content within a PVDF polymer, based on infrared spectroscopy and X-ray diffractometry data.

Please do not adjust margins

electrochemical stability (up to 4.5 V vs. Li/Li$^+$), high dielectric constant (>10 for β-phase), that facilitates the dissociation of lithium salts [18–20]. However, PVDF have low ionic conductivity because their ordered structure does not allow ions to migration through polymer matrix. Ionic conductivity can be found in amorphous regions of the polymer structure, where the polymer chains have segmental mobility[21]. To address this issue, we propose introducing an amorphous, thermoplastic polysulfone (PSF) into the PVDF-based system. This addition will reduce the crystallinity of the polymer blends and enhance ion conductivity. The presence of sulfonic groups may also contribute to increased ionic conductivity.

The incorporation of nanoparticles into a polymer-salt matrix is a well-established strategy for enhancing electrochemical and mechanical properties, as well as improving interfacial stability. Various ceramic fillers, such as TiO_2, Al_2O_3, MgO, etc. have been extensively studied for their effects on SPE properties. These nanoparticles not only act as plasticizers, suppressing polymer crystallization, but they also modulate cation mobility. Ceramic additives have two main effects: they act as cross-linking sites for both polymer chains and anions, preventing polymer recrystallization and promoting structural modifications. They also facilitate the formation of Li$^+$ transport pathways along the filler surfaces. As Lewis acid-based interaction sites with electrolyte ionic species, these fillers weaken the associations between anion-Li$^+$, facilitating the dissociation of the salt [20,22–24].

The interaction of charged particles, beyond Lewis's acid-base theory can also be described using the space-charge model. The presence of grain boundaries in the material promotes the partial migration of mobile charges to the boundary region where they accumulate, forming the so-called space-charge zone [25–28]. Conductivity in this carrier-rich space-charge zone is significantly higher than that in the bulk material. This theoretically leads to an increase in conductivity as the particle size decreases in nanocrystalline materials [29].

A wide range of studies on Li$^+$-ion and electron transport in bulk TiO_2 have shown that ions primarily move through interstitial sites, while electrons hop along the metal lattice in small polaron [30–32]. Upon Li^+ insertion, electrons become localized on Ti^{4+} ions, as indicated by the appearance of Ti^{3+} states in X-ray photoelectron spectroscopy [33]. The strong attraction between Li^+ and the localized electrons suggests their correlated hopping as charge-neutral pairs. The energy barriers for ion and electrons migration depend on the crystal structure and direction of transport, and can be estimated from measured Li^+ mobilities in the lattice.

In this study, we attempted to combine two promising techniques by using a composite based on a solution of two polymers with the addition of inert titanium dioxide nanoparticles and investigated the effect of nanoscale particles on the electrochemical performance of the composite polymer electrolyte.

Experimental

Preparation of solutions

Mixed compositions based on amorphous thermoplastic polysulfone (PSF; granular, grade PSF-150; G.S. Petrov Institute of Plastics JSC, Russia) and semicrystalline polyvinylidene fluoride (PVDF; powder, grade Solef 5130; Solvay, Belgium) were prepared using N-methyl-2- pyrrolidone (NMP; Rushim LLC, Russia), with the additional of lithium perchlorate (anhydrous $LiCLO_4$; ORT Khimreaktivy LLC, Russia) and titanium dioxide (TiO_2 powder; Rushim LLC, Russia). To stabilize the TiO_2 particles in the solution and polymer composition, a dispersant-modified polyurethane solution (Disperbyk-185, BYK-Chemie GmbH, Germany) was employed.

Dispersions of various compositions based on PSF and PSF-PVDF were prepared using a vacuum mixer at 50-60 °C. First, lithium salt ($LiCLO_4$) was dissolved in NMP using an ultrasonic bath for 30 minutes. Then, polymers were individually dissolved in the resulting NMP-salt solution for 6-8 hours. The agitator speed varied from 150 rpm during the first 120 minutes to 400 rpm thereafter. The resulting homogeneous solutions were mixed together for another 3 hours at 400 rpm. Finally, 30% titanium dioxide dispersed in NMP was added and stirred for another 10 hours at 150 rpm. In this study, we focus on the use of a polymer mixture with a ratio of 80% PVDF to 20% PSF. The rationale for selecting this specific ratio is explained in the Supplementary information (Section 1, Figure S1).

Production of thin film

Thin composite films were produced using the MSK-AFA-III-VC-110/220 automated thin film deposition system (MIT Corporation, USA). Dispersions were applied to glass substrates using a squeegee (with a gap height of 150 μm) at a speed of 30 mm/min, and then dried at a temperature of 55 °C for 12 hours. The resulting films were further dried for an additional 12 hours in a vacuum oven set at 100 °C.

Preparation of TiO_2 dispersion

The dispersion of titanium dioxide nanoparticles was prepared in NMP using a LabStar laboratory bead mill (Netzsch GmbH, Germany). Grinding was performed for 6 hours using 0.2 mm beads. Particle size was measured using the Zetasizer Nano ZS dynamic light scattering system (Malvern Panalytical, UK). Glass cells were used for the measurements. The dispersion was previously diluted about 1000 times in NMP.

Scanning electron microscopy

Cross sections of composite films were analyzed using a MIRA 3 LMU analytical scanning electron microscope (Tescan, Czech Republic) to evaluate the distribution of components within the material. The measurements were carried out at an accelerating voltage of 10 kV using a backscattered electron detector and an energy-dispersive spectrometer (EDS) to analyze the elemental composition of the films.

IR spectroscopy

The possible formation of chemical bonds during the mixing of components in the resulted polymer films was investigated using an IFS 66 v/s FTIR spectrometer (Bruker, Germany). Spectra were recorded using the NPV method with an accessory

 This journal is © The Royal Society of Chemistry 20xx

Please do not adjust margins

Please do not adjust margins

fitted with a $ZnSe$ crystal. The parameters used were: resolution 2 cm^{-1}, range 4000–600 cm^{-1}, 30 scans.

X-ray diffraction analysis

A TD-3700 X-ray diffractometer (Dandong Tongda Science & Technology Co., Ltd., China) was used to analyze the matrix and composite crystallinity. The X-ray measurements were taken in continuous θ–2θ mode between 3–45° 2θ with a step size of 0.02°. Additional information on lithium–polymer complex formation was obtained using a PHOIBOS HSA3500 CCD 225 R6-HiRes high-vacuum electron-ion spectroscopy system.

Electrochemical measurements

Electrochemical analysis of the composite films was carried out using a modular potentiostat/galvanostat PGSTAT 302 (Eco Chemie B.V., The Netherlands) and a multichannel potentiostat/galvanostat P-20X8 (Electrochemical Instruments, Russia). To determine ionic conductivity, samples were placed between two blocking steel electrodes and a potential difference (ΔV = 0.01 V) was applied, while recording impedance changes within the frequency range of 100 kHz to 0.1 Hz (5 points per decade) in Nyquist coordinates at temperatures ranging from 25 to 80 °C.

The LiFePO4 (LFP, BTR New Energy Materials, Shenzhen, China) based cathode was prepared by a mixture of LiFePO4: poly(vinylidene fluoride): Carbon black (Super P) at ratio 85:10:5 (wt.%) in NMP (Acros Organics, Geel, Belgium). The prepared electrode slurry was applied to a carbon-coated aluminum current collector with an applicator following the doctor-blade method and leaving a casting gap of 200 µm. After drying at 60°C, the sheet was roll-pressed with a roll gap and stamped into disk electrodes with an area of 2 cm^2. The electrodes were weighed and dried at 110°C in a vacuum (0.01 atm) overnight. Galvanostatic charge/discharge experiments were carried out in the potential range of 2.0–4.1 V vs. Li/Li^+. Specific capacities were normalized to the mass of the active material (LFP).

Result and discussion

Distribution of titanium oxide particles in the polymer matrix

The initial goal of this project was to investigate the characteristics of titanium dioxide nanoparticles after they were reduced to nanoscale using milling, and then to stabilize them in order to prevent aggregation and sedimentation. Figure 1 shows the X-ray diffraction pattern and SEM image of titanium dioxide powder used as a filler.

Strong diffraction peaks at 27°, 46° and 55° unambiguously confirm the presence of titanium dioxide in the rutile phase (Fig.1a)[32,34,35]. The phase barrier for lithium-ion transport in rutile is extremely low, on the order of 0.04 eV (c-direction)[36]. Incorporating titanium dioxide into the polymer electrolyte is expected to enhance its ionic conductivity.

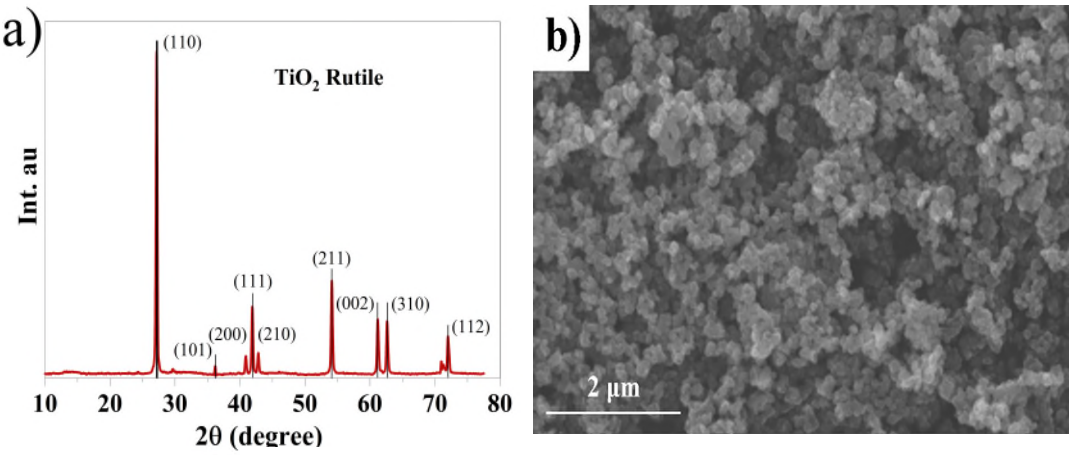


Figure 1 - X-ray diffraction (a) and SEM image (b) of titanium dioxide powder

The SEM image shows nanoparticles of titanium dioxide about 250 nm in size (Fig. 1b). Next, the particle-size distribution in the solvent after milling in a bead mill was determined (Figure 2a and Table 1). The data show an average particle size of approximately 225 nm, while the high polydispersity index indicates the presence of larger particles - up to 1 µm. Figure 2a also illustrates the sedimentation process, which shifts of the size distribution toward smaller diameters in sequential experiments.

To stabilize the particles in the solvent and to estimate their actual size, a surfactant was used at a concentration of 5 wt. % relative to titanium dioxide in the dispersion. The distribution of titanium dioxide particles in the dispersion with dispersant was investigated via dynamic light scattering. The results are shown in Figure 2b and Table 1.

Table 1 - Distribution of titanium dioxide particles after milling and adding dispersant

System	Z-average, nm	SD	Pd, %	Di %, nm
After milling	224.6	83	32.1	Di_{50} 243 Di_{90} 372
With dispersant	129.1	30.1	21.1	Di_{50} 136 Di_{50} 187

The results show that the use of the dispersant significantly reduces the signal distribution and decreases the particle size to 130 nm. This is evident from the lower average particle size and the low polydispersity, indicating minimal aggregation and sedimentation. «Measurement number» in Figure 2 refers to

Please do not adjust margins

Please do not adjust margins

the successive measurements carried out during the study of the systems.

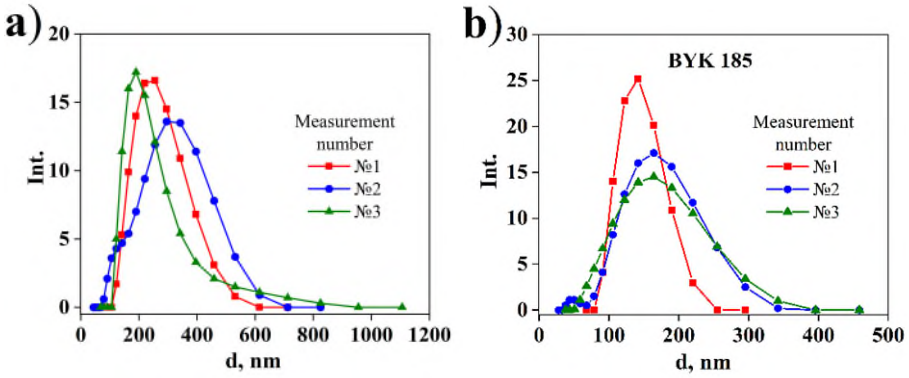


Figure 2 - Distribution of titanium oxide nanoparticles: a) after grinding in a bead mill and b) after added dispersant «BYK 185».

In order to confirm the effectiveness of a dispersant when titanium dioxide is added to a polymer matrix, a polysulfone-based model system was prepared. The film was made using a solution of 30 wt. % PSF in NMP with 5 wt. % titanium dioxide dispersion in NMP added. The dispersant concentration was also 5% of the mass of titanium particles (which corresponds to the manufacturer's recommendations).

The results of titanium dioxide distribution are presented as in the form of electronic spectra of characteristic titanium radiation from the cross-section of the polymer films (Figure S2a, c in Supplementary information). Intense signals in the range of up to 45 microns indicate the active aggregation of inorganic particles within the polymer matrix (Figure S2a Supplementary information). A quantitative evaluation was performed using Fourier transform signal analysis. These data show that the distribution of particles in films strongly depends on the presence of dispersant.

The Fourier transform provides insight into the frequency distribution of concentrations. Analysis of Figure S2 in Supplementary information reveals that disperse achieves the desired change in titanium distribution in the polymer film. This is evident from the narrow frequency distribution of peaks (indicated by the oval area on the graphs on the right). In other words, disperbyk 185 yields a statistically uniform distribution of titanium particles in the polymer film.

Therefore, it has been found that the use of a dispersant is justified, even if titanium dioxide is used in the form of a dispersion in a polymer matrix. The distribution of titanium particles remains uniform, which should positively affect the electrochemical properties of the polymer electrolyte.

FTIR spectrum of polymer matrix

To study the interaction of components in mixed compositions, a detailed structural analysis was carried out using FT-IR spectroscopy on thin films. Figure 3 present the FT-

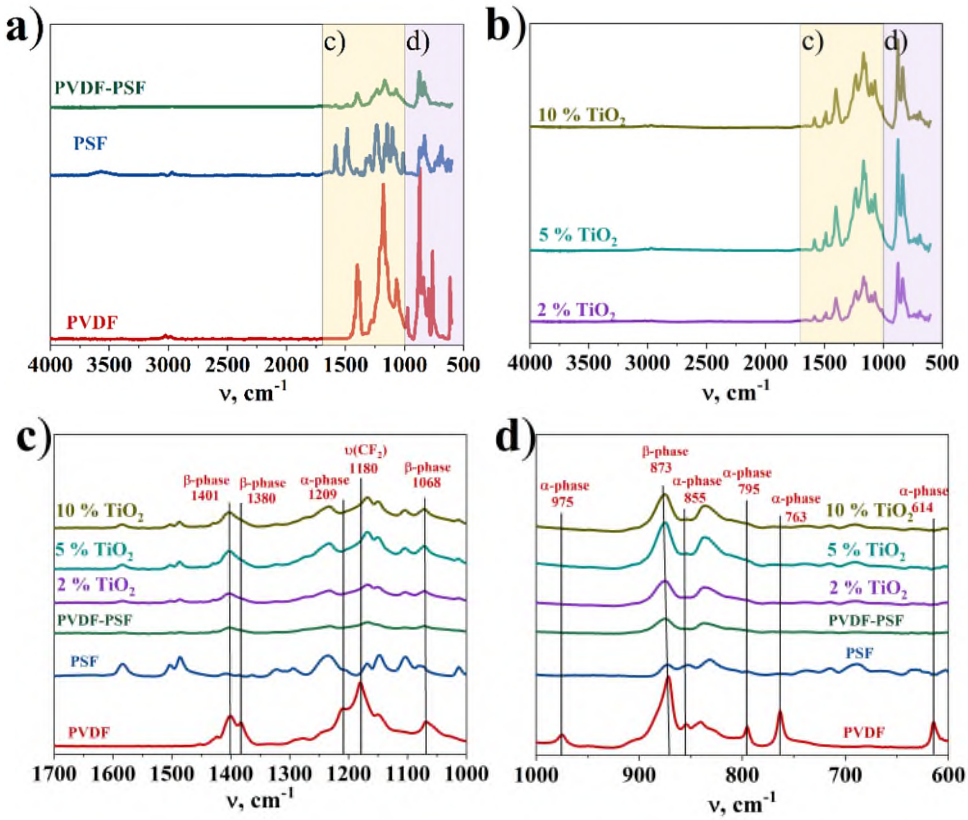


Figure 3 - FT-IR spectrum of a) PVDF, PSF and mixture PVDF and PSF films with lithium salt, b) composite films PVDF-PSF with 2, 5 and 10 % of TiO_2, c) all films range from 1700 to 1000 cm^{-1}, d) all films range from 1000 to 600 cm^{-1}

This journal is © The Royal Society of Chemistry 20xx

Please do not adjust margins

Please do not adjust margins

IR spectra PVDF-PSF polymer electrolyte with different content of TiO2.

The polysulfone spectrum corresponds well with that of commercial polysulfone (CAS No. 25135 51 7). Valency C=C vibrations and aromatic ring modes appear at 1584 and 1486 cm-1; C–H deformation vibrations of the aromatic ring appear at 836, 856, and 876 cm-1. Sulfone groups' symmetric S=O vibrations occur at 1320, 1295, 1148, and 1108 cm-1. The isopropylidene skeletal C–C vibrations are observed at 1020 cm-1, and Ph–O–Ph vibrations at 1235 cm-1.

The studied PVDF spectrum is in good agreement with literature data and has been the subject of close investigation [37–39]. Since several crystalline phases can exist in the polymer, the main ones being the nonpolar α-phase and the polar β-phase. It was established [40] that each phase has specific bands that can be present in the polymer.

IR spectra of mixed compositions

Reducing the crystallinity of PVDF while promoting phase redistribution is essential for polymer electrolytes, as ion transport occurs primarily in amorphous regions. Figures 4c and 4d compare the spectra of amorphous PSF, semi-crystalline PVDF, and composite films containing TiO_2 and $LiClO_4$. The addition of amorphous PSF and nanoscale TiO_2 leads to significant changes in the phase: α-phase bands at 1209, 975, 855, 795, 763, and 614 cm^{-1} almost disappear; β-phase bands at 1401 and 873 cm^{-1} decrease in intensity. The 1380 cm^{-1} shoulder is also smoothed, indicating a reduction in overall crystallinity.

The shifts in the peaks of PVDF at 1180, 1068, and 873 cm^{-1}, as well as the peak of PSF at 836 cm^{-1}, suggest the formation of complexes with Li^+ ions. Therefore, the incorporating of amorphous polymers and ceramic nanoparticles reduces the PVDF crystallinity while relatively increasing its polar crystalline phase, which should improve ionic conduction.

To quantify the content of each phase, a mathematical equation based on the Bouguer-Lambert-Beer law is used. This equation is presented in the Supplementary information (Section 3.1).

Based on the provided equation, it has been determined that the β-phase content of the PVDF-based film under study is approximately 35%. This is a relatively low value considering that polar phases are known to promote high ionic conductivity. However, this is a rather low value since it is the presence of these polar phases that ensure high levels of ionic conductivity.

Analyzing the spectra of all systems revealed a shift and redistribution of peak intensities within the PVDF matrix. This phenomenon is attributed to the addition of polysulfone, which induces a significantly increased the β-phase content from 35% to 86% (this was calculated with using equation (2) in Supplementary information). The increase in β-phase content can be explained by polysulfone ability to increase the system's viscosity. This hinders solvent evaporation during film formation. The elevated viscosity restricts the segmental mobility of the PVDF chains, preventing their reorganization and packing into the dense α-phase. At the same time, interactions between PVDF-PSF chains, including dipole-dipole and van der Waals forces, help stabilize the extended conformation of β-phase. In contrast, adding of titanium dioxide did not significantly alter the β-phase content. At concentrations of 2%, 5%, and 10%, the β-phase were 85%, 82%, and 79% a respectively.

X-Ray spectrum of polymer matrix

Figure 4 shows the XRD patterns of PVDF powder, PVDF film (cast from 10 wt. % solution) and composite films (titanium dioxide content increases in the direction of the arrow). The PVDF powder sample predominantly exhibits the α-phase, as shown by intense peaks at 18.3° and 20° and a shoulder at 26.6°, which correspond to the (020), (110), and (021) reflections of the monoclinic α-PVDF phase. Additional α-phase reflections appear at 32.2° (130), 35.9° (200), and 38.8° (002).

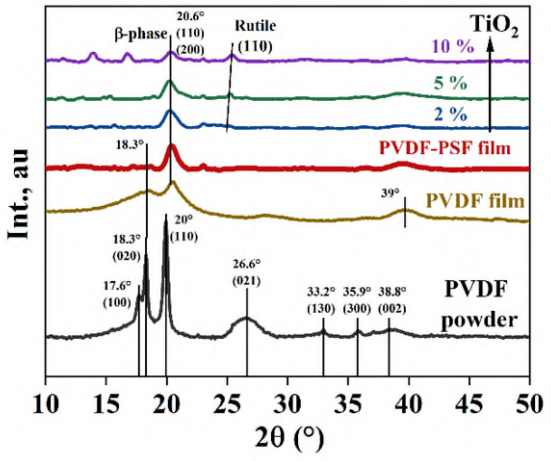


Figure 4 - Diffractogram of the studied compositions.

When examining PVDF films with different composite compositions, the changes is observed. The shear forces applied during film casting and subsequent drying lead to an almost complete disappearance of the α-phase. Instead, broad peaks are observed at 18.3° and 39°. At the same time, a clear transition from the α-phase to the β-phase is observed (20° → 20.6°) in good agreement with literature data [41,42].

The addition of PSF to the PVDF matrix results in an even stronger suppression of the α-phase peaks. A distinct peak at 20.6° corresponds to the (110)/(200) reflections of the orthorhombic β-phase. The incorporation of TiO_2 yields a low-intensity rutile peak around 25°. The interaction between nanoscale TiO_2 and the polymer matrix weakens intermolecular polymer–polymer interactions, reducing overall crystallinity. This effect is most pronounced in the 35–42° region, where increasing TiO_2 concentration suppresses the α-phase reflections at 35.9° and 38.8°. It is likely that Lewis's acid–base interactions between Ti^{4+} sites on TiO_2 and polymer –F groups hinder polymer chain mobility, thereby decreasing film crystallinity.

No diffraction peaks attributable to $LiClO_4$ are observed, suggesting that the salt is well dissociated and dispersed, forming complexes with the polymer matrix rather than existing as a separate crystalline phase.

The degree of crystallinity (common value and for β-phase) for PVDF powder, film and composite films was calculated using

Please do not adjust margins

Please do not adjust margins

the deconvoluting the XRD profile. Equations presented in Supplementary information (Section 3.2). Using these equations, it was determined that the degree of crystallinity of the PVDF film was not changed compared to the original PVDF powder (75% and 73%, respectively). However, the addition of PSF resulted in a significant decrease in the crystallinity of the polymer system (from 73% to 53%), which was expected due to the influence of amorphous polymers that hinder the crystallization process. These results were consistent with the IR spectroscopy data (Fig.3), which showed that the addition of PSF increased the content of the β-phase by approximately twofold (from 34% to 71%).

The influence of titanium dioxide on the distribution of the polymer phases

It is important to evaluate the distribution of the second phase (PSF) in the PVDF matrix as the titanium dioxide content changes (at constant $LiClO_4$ concentration). Figure 5 shows an SEM image of a film without TiO_2, where PSF forms a separate phase in the form of large, elongated droplets up to 40 μm in length. Their orientation reflects the shear flow during coating process.

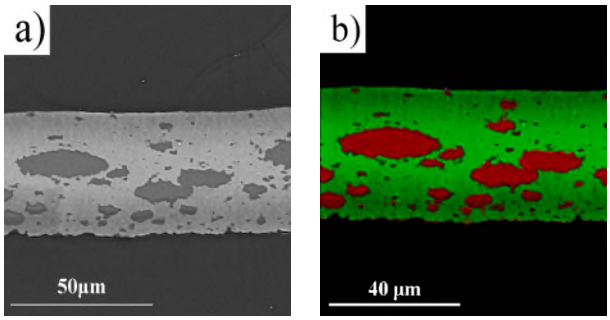


Figure 6 - a) SEM image of a section of 80% PVDF, 20% PSF film without TiO_2; b) color image of polymer distribution in the film. Red areas correspond to PSF, green – to PVDF.

The addition of TiO_2 significantly alters the components distribution. As shown in Figure 6, even at a 2 wt. % TiO_2 concentration, the average droplet size decreases from 40 μm to about 10 μm, indicating that TiO_2 acts as a compatibilizer, promoting PSF dispersion - effectively acting as a surfactant by interacting with the PSF. However, beyond a certain concentration of TiO_2 (around 10 wt%), PSF coalescence occurs

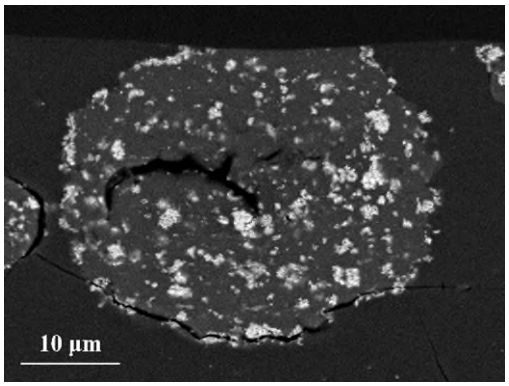


Figure 7 - SEM image of films of 20 % PVDF and 80 % PSF with 5 % TiO_2

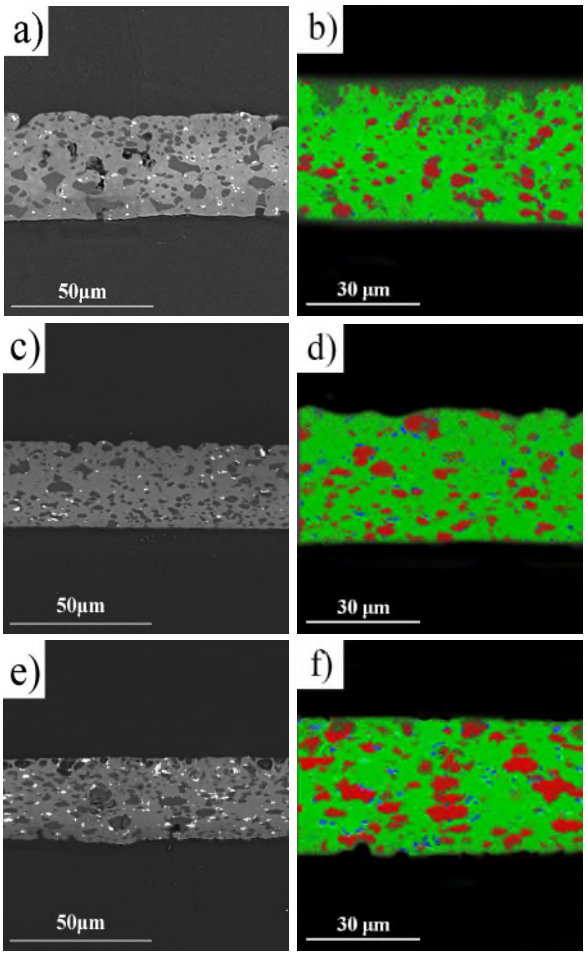


Figure 5 - a, c, d) SEM images and b, d, e) color images of sections of films of 80% PVDF and 20% PSF composition. a, b) with the addition of 2% TiO_2, c, d) 5% TiO_2, d, e) 10% TiO_2. Red areas correspond to PSF, green – PVDF, blue – titanium

and droplet sizes become similar to those in TiO_2-free films. Moreover, the incorporation of TiO_2 leads to a rougher film surface morphology, with regions of polymer partially localized at the interface between polymer–polymer, which could theoretically enhance the adhesion between the anode and cathode materials to the polymer electrolyte.

It is also worth noting that the dispersion of titanium dioxide particles can only be observed within the PVDF phase. This is especially evident in the model system (with a polymer ratio of 20 % PVDF and 80 % PSF) shown in Figure 7, where the titanium particles are predominantly distributed throughout the bulk of the PVDF and at the interface between the two polymers. In theory, this should improve the stability of the system given the initial state of immiscibility between the polymers.

Additional experiments on the quantitative distribution of PSF in a composite polymer electrolyte are presented in Figure S.3.

Electrochemistry of polymer systems

Impedance hodographs in Nyquist coordinates were obtained for all studied compositions, and ionic conductivity values were determined according to established theory. As shown in Figure 8, the addition of TiO_2 as a dopant significantly

This journal is © The Royal Society of Chemistry 20xx

Please do not adjust margins

increases ion conductivity: with increasing TiO_2 content up 10 10 wt.%, conductivity increases by approximately one and a half orders of magnitude.

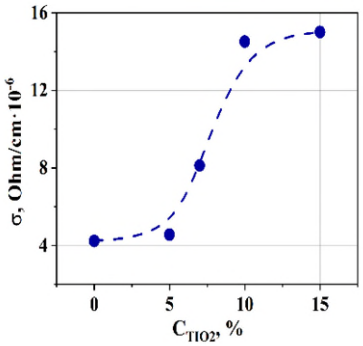


Figure 8 - Dependence of polymer electrolyte conductivity on titanium dioxide content

However, beyond a certain concentration of TiO_2, further increases (up to 15 wt.%) yield only marginal increases in conductivity and negatively affect film morphology due to the coalescence of the secondary polymer phase. These findings are correlate well with literature reports for TiO_2, Al_2O_2, and SiO_2 dopants [22,43–45].

To confirm this trend, temperature–dependent conductivity measurements were performed for all compositions (Figure 9). The resulting curves follow the Arrhenius relationship:

$$\sigma = \sigma_0 \, exp\left(\frac{-E_a}{k_B T}\right) \quad (1)$$

$$E_a = -\alpha_{1/T} \cdot 2.303 \cdot k_B \quad (2)$$

where E_a is the activation energy for Li^+ migration, k_B is the Boltzmann constant, $\alpha_{1/T}$ is the slope of the $1/T$ plot, and the factor 2.303 is the conversion coefficient. Table 2 summarizes the activation energies extracted from these plots.

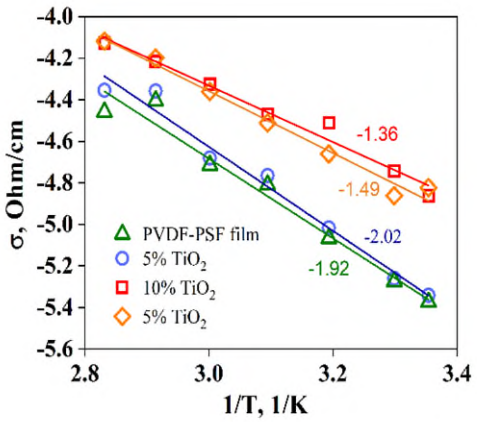


Figure 9 - Temperature dependence of conductivity in Arrhenius coordinates

Deviations from linearity at higher temperatures suggest the presence of an additional conduction mechanism, related to the motion of polymer segments above the glass transition of PVDF's, as a described by the Vogel–Tammann–Fulcher model.

Table 2 – Activation energy dependence of concentration of TiO_2

Concentration of TiO_2, %	Slope	E_a, eV
0	-1.9	0.38
5	-2.0	0.40
10	-1.4	0.27
15	-1.5	0.30

Among the samples, the composition containing 10 wt. % TiO_2 exhibits the lowest activation energy and the highest ionic conductivity, indicating it as the optimal doping concentration. This data correlates well with the values reported in the literature [46–50].

An interesting effect was observed during thermal cycling. When heating a film, its conductivity increased as expected. However, after cooling the cells for two hours and re-measuring impedance again, the conductivity remained high - even after further verification at 7 and 20 days (Figure 10). This sustained

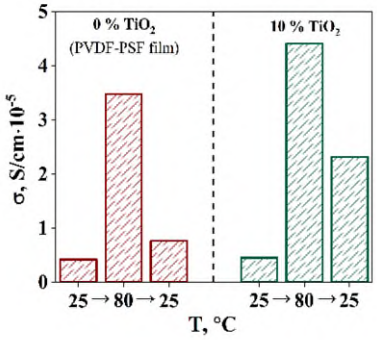


Figure 10 - Change in ion conductivity of polymer electrolyte films before/after heating.

conductivity increase may be due to a partial α→β phase transformation in the PVDF matrix. The exact mechanism remains to be determined.

Please do not adjust margins

Finally, the electrochemical performance of a 10 wt. % TiO_2 sample was evaluated at various charge/discharge rates (Figure 11). At low rates, the film's ionic conductivity was sufficient to support efficient electrochemical reactions. The LFP//PVDF/PSF/TiO2//Li cell shows superior rate performance with capacities of 149, 147, 138 and 123 mAh/g for C/5, C/3, C/2

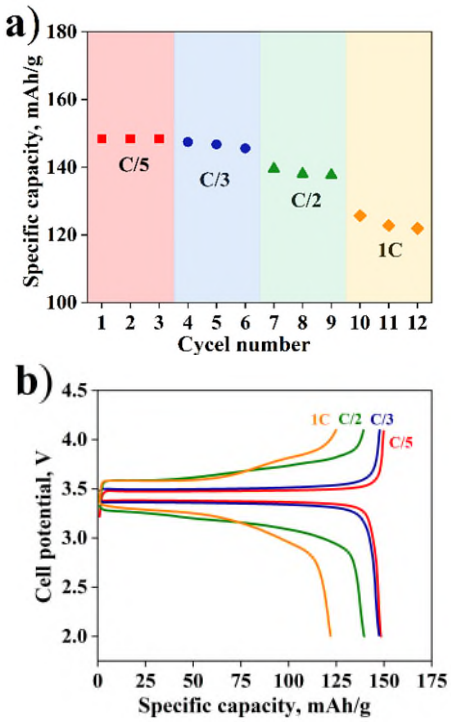


Figure 11 - a) Specific capacity at different charge/discharge currents; b) galvanostatic charge/discharge curves

and 1C respectively. These values were obtained at room temperature, which as a very high capacity for solid-state lithium-ion batteries.

Figure 11b shows the initial charge-discharge curve of the LFP//PVDF/PSF/TiO2//Li cell at different C-rate. As the current rate increases, the polarization voltage increases slightly. The rate capacity of this SPE is superior to or equal to than that of other SPEs based on PVDF electrolytes reported previously [18,46,51,52]. This suggests that this type of SPE membrane has great potential for future use in high-performance solid-state lithium metal batteries.

Conclusions

A detailed study was conducted to investigate the effect of nanoscale titanium dioxide ceramic particles on the electrochemical properties of a polymer electrolyte made from a mixture of PVDF and PSF polymers. It was found that the addition of TiO2 particles increased the ion conductivity of the composite film by about an order of magnitude (up to $4 \cdot 10^{-5}$ S/cm). However, this effect decreased when the concentration of ceramic particles exceeded a certain critical level (10 wt.%).

Additionally, it was surprising to find that titanium particles act as a compatibilizer, improving the interface between the two immiscible polymers and leading to a more uniform distribution of the PSF phases within the PVDF matrix. Moreover, the addition of ceramic particles also reduced the size of the second PSF-phase in the system, potentially enhancing the mechanical and electrochemical properties. These findings provide additional motivation for research into polymer mixtures that can be used as solid polymer electrolytes.

The developed composite polymer electrolyte has been successfully tested in cycling of solid-state metal-ion battery. At a current density of C/5, the discharge capacity was 149 mAh/g, which is a very promising value for solid-state devices operating at room temperature.

Conflicts of interest

There are no conflicts to declare.

Acknowledgements

This work was carried out within the State Program of TIPS RAS.

References

1 D. Chen, Z. Zhou, C. Feng, W. Lv, Z. Wei, K. H. L. Zhang, B. Lin, S. Wu, T. Lei, X. Guo, G. Zhu, X. Jian, J. Xiong, E. Traversa, S. X. Dou and W. He, *Advanced Energy Materials*, 2019, **9**, 1803627.
2 C. M. Costa, Y.-H. Lee, J.-H. Kim, S.-Y. Lee and S. Lanceros-Méndez, *Energy Storage Materials*, 2019, **22**, 346–375.
3 X. Zhou, Z. Fan, Y. Ma and Z. Gao, in *2017 36th Chinese Control Conference (CCC)*, 2017, pp. 10674–10678.
4 X. Dai, X. Zhang, J. Wen, C. Wang, X. Ma, Y. Yang, G. Huang, H.-M. Ye and S. Xu, *Energy Storage Materials*, 2022, **51**, 638–659.
5 W. Xie, X. Liu, R. He, Y. Li, X. Gao, X. Li, Z. Peng, S. Feng, X. Feng and S. Yang, *Journal of Energy Storage*, 2020, **32**, 101837.
6 A. Masias, J. Marcicki and W. A. Paxton, *ACS Energy Lett.*, 2021, **6**, 621–630.
7 Y. Liu, Q. Duan, J. Xu, H. Chen, W. Lu and Q. Wang, *RSC Adv.*, 2018, **8**, 42223–42232.
8 E. P. Roth and C. J. Orendorff, *Electrochem. Soc. Interface*, 2012, **21**, 45.
9 W. Liu, M.-S. Song, B. Kong and Y. Cui, *Adv Mater*, DOI:10.1002/adma.201603436.
10 S. Chen, K. Wen, J. Fan, Y. Bando and D. Golberg, *J. Mater. Chem. A*, 2018, **6**, 11631–11663.
11 G. Zhou, F. Li and H.-M. Cheng, *Energy Environ. Sci.*, 2014, **7**, 1307–1338.
12 D. Zhou, A. Tkacheva, X. Tang, B. Sun, D. Shanmukaraj, P. Li, F. Zhang, M. Armand and G. Wang, *Angew Chem Int Ed Engl*, 2019, **58**, 6001–6006.
13 N. Yazie, D. Worku, N. Gabbiye, A. Alemayehu, Z. Getahun and M. Dagnew, *Mater Renew Sustain Energy*, 2023, **12**, 73–94.
14 A. S. Aricò, P. Bruce, B. Scrosati, J.-M. Tarascon and W. van Schalkwijk, *Nat Mater*, 2005, **4**, 366–377.
15 B. G. Westphal, N. Mainusch, C. Meyer, W. Haselrieder, M. Indrikova, P. Titscher, H. Bockholt, W. Viöl and A. Kwade, *Journal of Energy Storage*, 2017, **11**, 76–85.
16 N. García, J. Guzman, P. Tiemblo and A. Mejía, *Electrochimica Acta*, 2014, **137**, 526–534.

This journal is © The Royal Society of Chemistry 20xx

Please do not adjust margins

Please do not adjust margins

17 A. Karim, D.-W. Liu, J. F. Douglas, A. I. Nakatani and E. J. Amis, *Polymer*, 2000, **41**, 8455–8458.
18 Y. Wu, Y. Li, Y. Wang, Q. Liu, Q. Chen and M. Chen, *Journal of Energy Chemistry*, 2022, **64**, 62–84.
19 H. Xie, Z. Tang, Z. Li, Y. He, Y. Liu and H. Wang, *J Solid State Electrochem*, 2008, **12**, 1497–1502.
20 J. Vicente, P. Costa, S. Lanceros-Mendez, J. M. Abete and A. Iturrospe, *Materials (Basel)*, 2019, **12**, 3545.
21 S. Abbrent, J. Plestil, D. Hlavata, J. Lindgren, J. Tegenfeldt and Å. Wendsjö, *Polymer*, 2001, **42**, 1407–1416.
22 K. K. Ganta, V. R. Jeedi, V. K. Katrapally, M. Yalla and L. N. Emmadi, *J Inorg Organomet Polym*, 2021, **31**, 3430–3440.
23 M. Jagan and S. P. Vijayachamundeeswari, *Ionics*, 2024, **30**, 647–675.
24 M. L. Sushko, K. M. Rosso and J. Liu, *J. Phys. Chem. C*, 2010, **114**, 20277–20283.
25 J. U. Ha, J. Lee, M. A. Abbas, M. D. Lee, J. Lee and J. H. Bang, *ACS Appl. Mater. Interfaces*, 2019, **11**, 11391–11402.
26 S. Huang, Y. Fang, B. Wang, B. E. Wilson, N. Tran, D. G. Truhlar and A. Stein, *J. Phys. Chem. C*, 2016, **120**, 9637–9649.
27 X. Yang, Y. Yang, H. Hou, Y. Zhang, L. Fang, J. Chen and X. Ji, *J. Phys. Chem. C*, 2015, **119**, 3923–3930.
28 M. N. Hyder, B. M. Gallant, N. J. Shah, Y. Shao-Horn and P. T. Hammond, *Nano Lett.*, 2013, **13**, 4610–4619.
29 S. Hu, Y. Li, K. M. Rosso and M. L. Sushko, *J. Phys. Chem. C*, 2013, **117**, 28–40.
30 M. Zhu, B. Yu, W. Cui, Y. Sun and M. Ma, *Journal of Power Sources*, 2024, **622**, 235363.
31 S. Soltani, M. Ardyanian and M. M. Shahidi, *Optical Materials*, 2024, **152**, 115484.
32 X. Wang, S. Liang, Y.-J. Cheng, Y. Xia and P. Müller-Buschbaum, *Renewable and Sustainable Energy Reviews*, 2025, **209**, 115101.
33 N. A. Deskins, P. M. Rao and M. Dupuis, in *Springer Handbook of Inorganic Photochemistry*, eds. D. Bahnemann and A. O. T. Patrocinio, Springer International Publishing, Cham, 2022, pp. 365–398.
34 M. M. El-Desoky, I. Morad, M. H. Wasfy and A. F. Mansour, *J Mater Sci: Mater Electron*, 2020, **31**, 17574–17584.
35 K. Thamaphat, P. Limsuwan and B. Ngotawornchai, .
36 M. V. Koudriachova, N. M. Harrison and S. W. de Leeuw, *Solid State Ionics*, 2003, **157**, 35–38.
37 L. Li, M. Zhang, M. Rong and W. Ruan, *RSC Adv.*, 2013, **4**, 3938–3943.
38 D. M. Dhevi, A. A. Prabu and K. J. Kim, *J Mater Sci*, 2016, **51**, 3619–3627.
39 J. Gomes, J. S. Nunes, V. Sencadas and S. Lanceros-Mendez, *Smart Mater. Struct.*, 2010, **19**, 065010.
40 X. Cai, T. Lei, D. Sun and L. Lin, *RSC Adv.*, 2017, **7**, 15382–15389.
41 P. Martins, A. C. Lopes and S. Lanceros-Mendez, *Progress in Polymer Science*, 2014, **39**, 683–706.
42 W.-Y. Chang, T.-H. Fang, S.-Y. Liu and Y.-C. Lin, *Materials Science and Engineering: A*, 2008, **480**, 477–482.
43 T. Regu, C. Ambika, K. Karuppasamy, J.-H. Jeon, Y.-T. Jeong, D. Vikraman, T. A. B. Raj and H.-S. Kim, *Ionics*, 2019, **25**, 5117–5129.
44 Z. Li, G. Su, D. Gao, X. Wang and X. Li, *Electrochimica Acta*, 2004, **49**, 4633–4639.
45 P. Singh and A. L. Saroj, *Polymer-Plastics Technology and Materials*, 2021, **60**, 298–305.
46 Z. Yao, F. Qi, L. Ye, Q. Sun, X. Gu, X. Yang and K. Zhu, *Heliyon*, 2024, **10**, e28097.
47 Q. Zhu, K. Yang, L. Chen, X. An, S. Guo, Y. Li, Y. Ma, Y. Cao, M. Liu and Y.-B. He, *Angewandte Chemie International Edition*, 2025, **64**, e202425221.
48 K. P. Radha, S. Selvasekarapandian, S. Karthikeyan and C. Sanjeeviraja, in *Solid State Ionics*, WORLD SCIENTIFIC, 2012, pp. 523–533.
49 F. Li, B. Su, L. Shi, J. Mu, F. Xu, J. Wang, H. Yang and Z. Guo, *Ceramics International*, 2023, **49**, 26604–26615.
50 L. Bai, X. Chen, F. Zhang, H. Zhou, Y. Li, P. Wang, N. Li and J. Xiao, *ACS Omega*, 2024, **9**, 31620–31630.
51 F. Wang, L. Li, X. Yang, J. You, Y. Xu, H. Wang, Y. Ma and G. Gao, *Sustainable Energy & Fuels*, 2018, **2**, 492–498.
52 B. Halder, M. G. Mohamed, S.-W. Kuo and P. Elumalai, *Materials Today Chemistry*, 2024, **36**, 101926.

This journal is © The Royal Society of Chemistry 20xx

Please do not adjust margins

Supplementary Files

This is a list of supplementary files associated with this preprint. Click to download.

- ArticleSupplementaryinformation.docx
- FigureS3.tif